Title

Field induced spontaneous quasiparticle decay and renormalization of quasiparticle dispersion in a quantum antiferromagnet

Authors

Hong, Tao
Qiu, Y
Matsumoto, M
et al.

Peer reviewed

Field-induced spontaneous quasiparticle decay and renormalization of quasiparticle dispersion in a quantum antiferromagnet

Tao Hong,[1, *] Y. Qiu,[2] M. Matsumoto,[3] D. A. Tennant,[1] K. Coester,[4] K. P. Schmidt,[5] F. F. Awwadi,[6] M. M. Turnbull,[7] H. Agrawal,[8] and A. L. Chernyshev[9]

[1]*Quantum Condensed Matter Division, Oak Ridge National Laboratory, Oak Ridge, Tennessee 37831, USA*
[2]*National Institute of Standards and Technology, Gaithersburg, Maryland 20899, USA*
[3]*Department of Physics, Shizuoka University, Shizuoka 422-8529, Japan*
[4]*Lehrstuhl für Theoretische Physik I, TU Dortmund, D-44221 Dortmund, Germany*
[5]*Lehrstuhl für Theoretische Physik I, Staudtstrasse 7,*
Universität Erlangen-Nürnberg, D-91058 Germany
[6]*Department of Chemistry, The University of Jordan, Amman 11942, Jordan*
[7]*Carlson School of Chemistry, Clark University, Worcester, Massachusetts 01610, USA*
[8]*Instrument and Source Division, Oak Ridge National Laboratory, Oak Ridge, Tennessee 37831, USA*
[9]*Department of Physics and Astronomy, University of California, Irvine, California 92697, USA*

The intrinsic zero-temperature damping in quantum spin systems is a spectacular quantum many-body effect, which is driven by the interaction of the one-magnon states and multi-magnon continuum. Here we present the high-resolution neutron scattering study of an ordered $S=1/2$ coupled two-leg ladder antiferromagnet (dimethylammonium)(3,5-dimethylpyridinium)CuBr$_4$ in applied magnetic fields and at temperature down to 0.1 K. Compared with the non-interacting linear spin-wave theory, our results demonstrate a variety of intriguing phenomena including field-induced renormalization of one-magnon dispersion, spontaneous magnon decay observed via intrinsic linewidth broadening, unusual non-Lorentzian two-peak structure in the excitation spectra, and dramatic shift of spectral weight from one-magnon state to the two-magnon continuum.

The notion of a quasiparticle, such as a phonon, a roton, or a magnon, is used in modern condensed matter physics to describe an elementary collective excitation. Naturally, quasiparticles are assumed to have long, or even infinite intrinsic lifetime, because of either the weak interactions or the prohibiting energy-momentum conservation for scatterings. However, this picture can break down spectacularly in some rare conditions. The quasiparticle decay was first predicted [1] and then discovered in the phonon-like excitation spectrum of the superfluid ^{4}He [2–4], where the phonon-like quasiparticle beyond a threshold momentum decays into two rotons. In magnetism, the spontaneous ($T=0$) magnon decays into the two-magnon continuum were observed by inelastic neutron scattering (INS) in zero field in various valence-bond type quantum spin systems including PHCC [5], IPA-CuCl$_3$ [6], and BiCu$_2$PO$_6$ [7] as well as in some triangular-lattice compounds [8, 9]. The mechanism for this magnon instability is the three-magnon scattering, which is enhanced in the vicinity of the threshold for the decays of one-magnon to two-magnon states [10–12].

By contrast, the phenomenon of the field-induced spontaneous magnon decay in ordered antiferromagnets (AFMs) is much less mature experimentally. Although the key three-magnon coupling term is forbidden for the collinear ground state, it is present in an applied magnetic field when spins are canted along the field direction, i.e., the coupling is facilitated via a field-induced spin noncollinearity. To date, spontaneous magnon decay in canted AFMs has been thoroughly studied theoretically [12–18], but there have been very few detailed experimental studies due to the lack of materials with suitable energy scales. The only experimental evidence was reported by Masuda *et al.* in an $S=5/2$ square-lattice AFM Ba$_2$MnGe$_2$O$_7$ [19], where the INS spectra become broadened in a rather narrow part of the Brillouin zone (BZ). For the quantum spin-1/2 systems, the magnon decay effect is expected to be much more pronounced, with the analytical [13, 14] and numerical studies [15, 16] predicting overdamped one-magnon excitations in a large part of the BZ.

We report the neutron scattering measurements on an $S=1/2$ quantum AFM (dimethylammonium)(3,5-dimethylpyridinium)CuBr$_4$ (C$_9$H$_{18}$N$_2$CuBr$_4$, abbreviated as DLCB) with an applied magnetic field up to 10.8 T. Figure 1(a) shows the molecular ladder structure of DLCB with the chain direction extending along the crystallographic **b** axis [20]. At zero field, the interladder coupling is sufficiently strong to drive the system into the ordered phase and the material orders magnetically at $T_N=1.99(2)$ K coexisting with a spin energy gap due to a small Ising anisotropy [21]. In finite fields, our study shows a strong evidence of the field-induced spontaneous magnon decay manifesting itself by the excitation linewidth broadening and by a dramatic loss of spectral weight, both of which are associated with the three-magnon interactions that lead to magnon spectrum renormalization and to the kinematically allowed one-magnon decays into the two-magnon continuum.
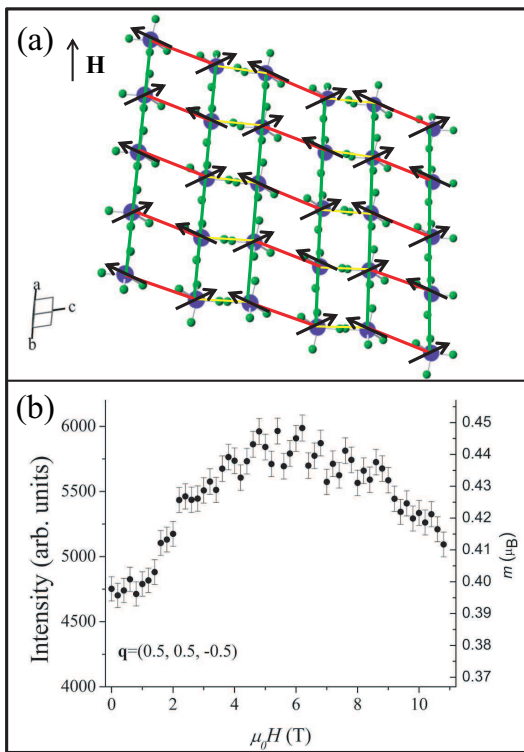
FIG. 1: **Canted spin structure of $S=1/2$ coupled two-leg spin ladders in an external magnetic field.** (a) Projection of $CuBr_4^{-2}$ tetrahedra showing the proposed 2D coupled two-leg ladders structure with the ladder chain along the **b** axis. Color coding of atoms is as follows: Blue: Cu and green: Br. Other atoms are omitted for clarity. Red, green, and yellow lines indicate the intraladder couplings J_{rung}, J_{leg}, and interladder coupling J_{int}, respectively. Black arrows indicate the canted spin structure in an external magnetic field applied along the $[1\ \bar{1}\ 0]$ direction in the real space. (b) Left: background-subtracted magnetic peak intensity of neutron scattering (right: the staggered moment) at **q**=(0.5, 0.5, −0.5) as a function of applied field measured at CTAX and T=0.25 K. Error bars represent one standard deviation determined assuming Poisson statistics.

FIG. 2: **False-color maps of the excitation spectra along two high-symmetry directions measured at DCS and T=0.1 K.** (a, b) $\mu_0 H$=0, (c, d) $\mu_0 H$=4 T, (e, f) $\mu_0 H$=6 T, and (g, h) $\mu_0 H$=10 T. The white arrows indicate renormalization of the TM_{high} mode. The red arrows indicate the experimental evidence of the TM_{low} mode. Red and yellow lines are LSW calculations of the acoustic TM_{high} and TM_{low} one-magnon dispersion, respectively. Grey lines are the calculated lower boundary of two-magnon continuum as described in the Methods.

Results

High-field neutron diffraction measurements. The magnetic structure at zero field is collinear with the staggered spin moments ($\sim$0.4 μ_B) aligned along an easy axis i.e. the **c*** axis in the reciprocal lattice space [21]. When a magnetic field is applied perpendicular to the easy axis, the ordered moments would cant gradually towards the field direction and saturate at $\mu_0 H_s \sim$16 T [22]. Figure 1(b) shows (left: the magnetic scattering intensity; right: size of the ordered staggered moment) measured at **q**=(0.5, 0.5, −0.5) and T=0.25 K as a function of field. The intensity initially grows due to the gradual suppression of quantum fluctuations with field and reaches a peak value around 6 T and then decreases with increase of the field because the spin canting angle
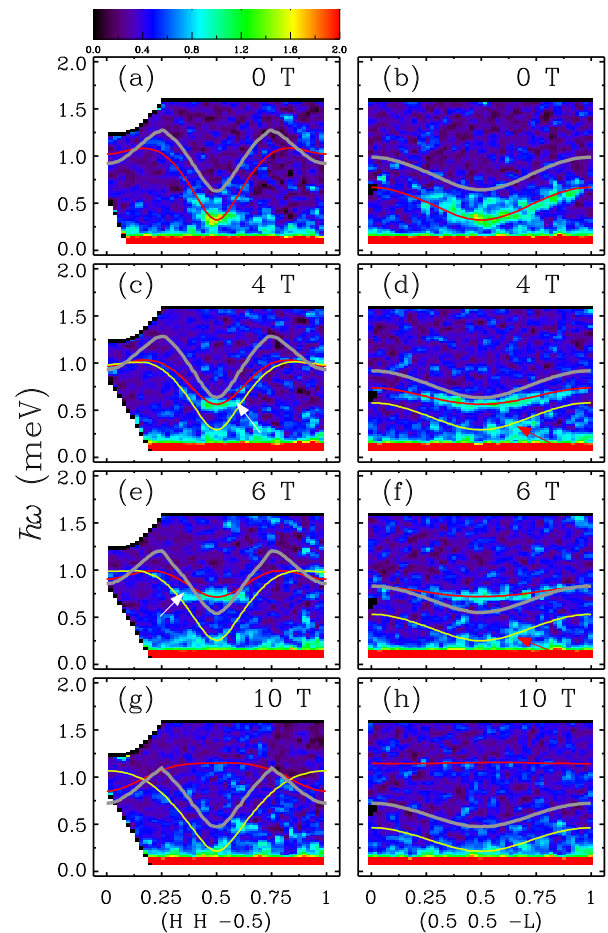
becomes large. There is no evidence of a phase transition confirming this semiclassical picture. Within the linear spin-wave theory, one may expect a similar semiclassical scenario to apply for the spin dynamics.

High-field inelastic neutron-scattering measurements. The spin dynamics, by contrast, undergoes a dramatic change with magnetic fields. Figure 2 shows false-color maps of the spin-wave spectra along two high-symmetry directions in the reciprocal lattice space measured at $\mu_0 H$=0, 4, 6, and 10 T and T=0.1 K. Spectral weights of the transverse optical branches are negligible in the current experimental configurations. As shown in Figs. 3(a) and (b), at zero field, the observed spin gapped magnetic excitation spectra agree well with the calcula-
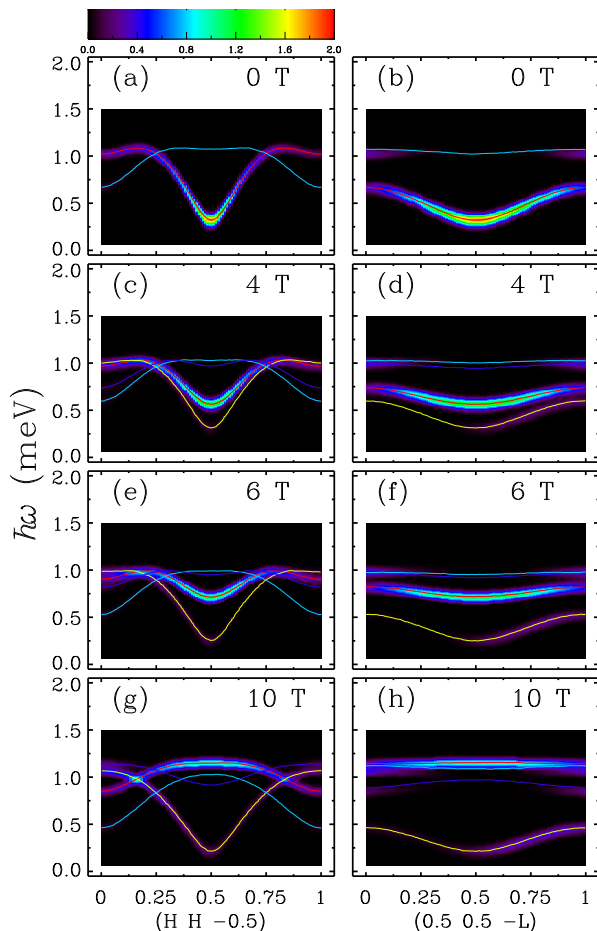
FIG. 3: **LSW calculations of the excitation spectra along two high-symmetry directions after convolved with the instrumental resolution function.** (a, b) $\mu_0 H=0$, (c, d) $\mu_0 H=4$ T, (e, f) $\mu_0 H=6$ T, and (g, h) $\mu_0 H=10$ T. The parameters of $J_{\mathrm{leg}}=0.60$ meV, $J_{\mathrm{rung}}=0.70$ meV, $J_{\mathrm{int}}=0.17$ meV, and an exchange anisotropy parameter $\lambda=0.95$ provide the best agreement with experimental data. The calculated intensity at each field was scaled against the total moment sum rule and the same way was also applied for calculations in Fig. 5(c). Red and yellow lines are the calculated acoustic TM_{high} and TM_{low} one-magnon dispersion, respectively. Blue and steelblue lines are the calculated optical TM_{high} and TM_{low} one-magnon dispersion, respectively.

tions using SPINW in linear spin-wave (LSW) approximation [23] convolved with the instrumental resolution function, as described in the Methods. At $H>0$, the transverse acoustic mode splits into two branches owing to the broken uniaxial symmetry. The high-energy mode (TM_{high}) corresponds to the spin fluctuations along the field direction. The low-energy mode (TM_{low}) corresponds to the spin fluctuations perpendicular to both the field direction and the staggered spin moment ($\equiv \hat{\mathbf{z}}$) and is indeed evidenced in Figs. 2(d) and (f) (pointed out by the red arrows). The dispersion bandwidths of the

TM_{high} mode collapse with field, which can also be captured at this LSW level. For instance, the bandwidths along the (H, H, -0.5) direction at $\mu_0 H=4$ and 6 T are reduced to 0.44 and 0.25 meV, respectively, from 0.80 meV at zero field. Surprisingly, however, we notice that TM_{high} mode near the BZ center in Figs. 2(c) and (e) visibly bends away from the quadratic LSW calculation in Figs. 3(c) and (e) for $\mu_0 H=4$ and 6 T (pointed out by the white arrows). Such a renormalization of one-magnon dispersion, which is attributed to the strongly repulsive interaction with the two-magnon continuum to avoid the overlap between them, was also recently reported in a different ladder compound, $BiCu_2PO_6$ [7]. Moreover, the spectral weight of one-magnon modes at $\mu_0 H=10$ T in Figs. 2(g) and (h) is much less than what is expected from the LSW theory in Figs. 3(g) and (h), indicative of a shift of the spectral weight from one-magon to multi-magnon continuum.

To investigate this quantum effect in more detail, we have measured excitations at the magnetic zone center $\mathbf{q}=(0.5, 0.5, -0.5)$ with field up to 10.8 T and $T=0.1$ K using a high-flux cold-neutron spectrometer. Figure 4(a) summarizes the background-subtracted field dependence of the magnetic excitations. Besides TM_{high} and TM_{low} modes, interestingly, there is also evidence of a mode (LM) which is is induced by the spin fluctuations along $\hat{\mathbf{z}}$ but not anticipated by LSW [24]. At zero field, it is called the longitudinal mode [25, 26], which is predicted to appear in quantum spin systems with a reduced moment size in a vicinity of a quantum critical point [27]. A detailed study of this type of excitation at zero field will be reported elsewhere.

Figure 4(b) shows the representative background-subtracted energy scans at the magnetic zone center in different fields. To extract the peak position Δ and the intrinsic (instrumental resolution corrected) excitation width Γ, we employed the same two-Lorentzian damped harmonic-oscillator (DHO) model in Eq. (1) as cross section used in our previous high-pressure studies [28, 29] and numerically convolved it with the instrumental resolution function as described in the Methods.

$$S(\omega) = \frac{A}{1 - \exp(-\hbar\omega/k_B T)}$$
$$\left[\frac{\Gamma}{(\hbar\omega - \Delta)^2 + \Gamma^2} - \frac{\Gamma}{(\hbar\omega + \Delta)^2 + \Gamma^2}\right]. \qquad (1)$$

The results are plotted in solid (dashed) lines shown in Fig. 4(b). The spectral line shape at zero field is the superposition of two such DHOs and the best fits gives location of two spin gaps at $\Delta_{\mathrm{TM}}=0.32(3)$ and $\Delta_{\mathrm{LM}}=0.48(3)$ meV, respectively. LM mode increases with field and is traceable up to 4 T. For TM_{high} mode, the observed peaks are instrumental resolution limited ($\Gamma \rightarrow 0$) up to 4 T although the lineshape looks narrow at 4 T due to the shallow dispersion slope. The steeper slope at zero field
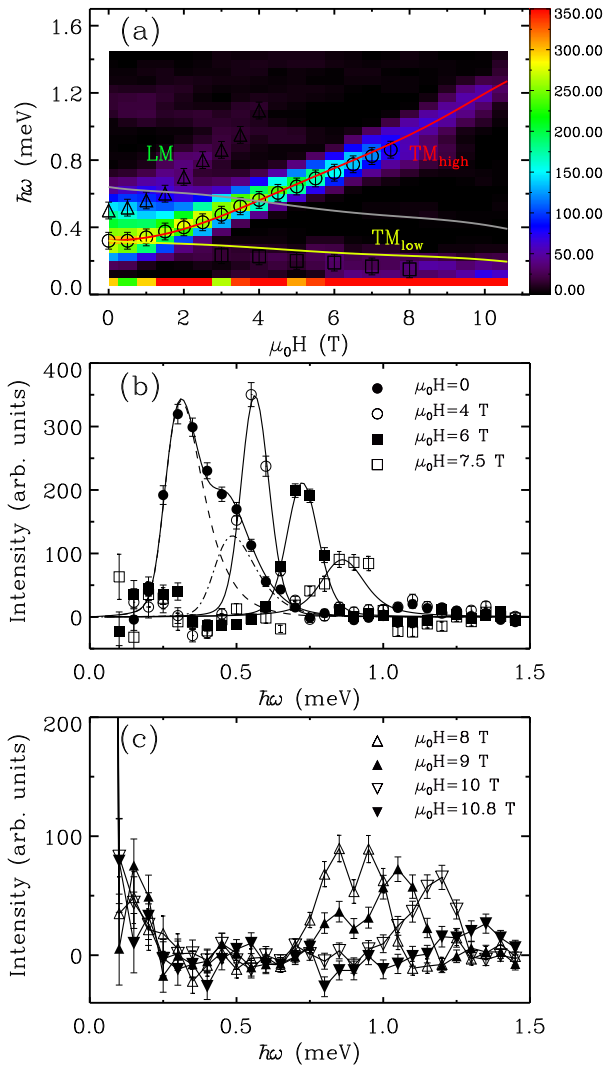
FIG. 4: **Evolution of magnetic excitation spectra at the magnetic zone center and $T=0.1$ K with magnetic field**. (a) False color neutron scattering intensity after background subtraction as a function of $\mu_0 H$ and $\hbar\omega$ measured at MACS. Circle, square, and triangle points are peak positions obtained from the fit as described in the text for TM_{high}, TM_{low}, and LM modes, respectively. Red and yellow lines are calculated by LSW. The grey line is the calculated lower boundary of two-magnon continuum; Representative background-subtracted energy scans at (b) $\mu_0 H=0$, 4, 6, and 7.5 T. The solid lines are calculations convolved with the instrumental resolution function. The dashed and dashed dotted lines are calculations for zero field TM_{high} and LM modes, respectively; (c) $\mu_0 H=8$, 9, 10, and 10.8 T. Each line is a guide for the eye. Error bars represent one standard deviation determined assuming Poisson statistics.

induces a broad peak due to the finite instrumental wave-vector resolution. At $\mu_0 H=6$ and 7.5 T, the line shapes become broadened and the best fits give full-width at half-maximum (FWHM) $2\Gamma=0.03(1)$ and $0.07(1)$ meV, respectively.

With further increase of field, the spectral line shape becomes complex. As shown in Fig. 4(c), the two-peak structures, distinct from the one-magnon state, appear in the spectrum and are accompanied by a suppression of the magnon intensity. These complex features are consistent with the theoretical prediction for spontaneous magnon decay and spectral weight redistribution at high fields [13, 18].
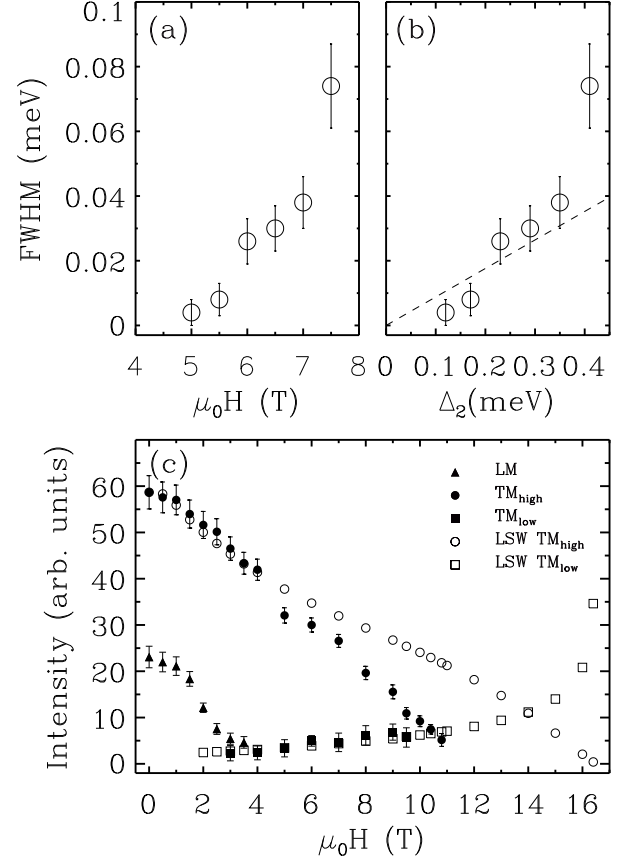

FIG. 5: **Evidences of spontaneous magnon decays at the magnetic zone center.** (a) Field and (b) Δ_2 dependence of intrinsic FWHM of magnon damping. The dashed line is a guide for the eye. (c) Field-dependence of energy-integrated intensity. Filled circle, square, and triangle points are the experimental data for TM_{high}, TM_{low}, and LM modes, respectively. Open circle and square points are calculations for TM_{high} and TM_{low} modes, respectively. Error bars represent one standard deviation determined assuming Poisson statistics.

Discussion

The observed magnon instability at finite fields originates from a hybridization of the single-magnon state with the two-magnon continuum. The process of one-magnon decays into two-magnon continuum is allowed if

the following kinematic conditions are satisfied:

$$\mathbf{q} = \mathbf{q}_1 + \mathbf{q}_2, \tag{2}$$
$$\varepsilon_2(\mathbf{q}) = \varepsilon_1(\mathbf{q}_1) + \varepsilon_1(\mathbf{q}_2), \tag{3}$$
$$\varepsilon_2(\mathbf{q})^{\min} \leq \varepsilon_1(\mathbf{q}) \leq \varepsilon_2(\mathbf{q})^{\max}, \tag{4}$$

where ε_1 is the one-magnon dispersion relation, and $\varepsilon_2^{\min}$ and $\varepsilon_2^{\max}$ are the lower and upper boundary of the two-magnon continuum, respectively.

Since S_z is not a good quantum spin number, the two-magnon continuum at finite field can be obtained from any combination between the acoustic and optical TM_{high} and TM_{low} modes. We calculated the lower boundary of two-magnon continuum, as described in the Methods, plotted as grey lines in Fig. 2 and Fig. 4(a). The upper boundary, which is above the experimental energy range, is not shown. At zero field and along the reciprocal lattice (H, H, -0.5) direction, the lower boundary already crosses over with TM_{high} mode at H′ ≈0.15 and 1-H′ ≈0.85, suggesting that DLCB is prone to magnon decays. Upon increase of the field, the lower boundary of two-magnon continuum decreases. Above 10 T, the continuum lies underneath the single-magnon branch for the whole BZ as shown in Figs. 2(g) and (h), so the effect of spontaneous decays is expected to be significant.

In the consideration of the magnetic zone center, the lower boundary of two-magnon continuum crosses over with the TM_{high} mode at 4 T as shown in Fig. 4(a). Figure 5(a) shows the derived intrinsic FWHM, characteristic of magnon damping, as a function of field up to 7.5 T for TM_{high} mode. The excitation spectra become even more broadening at higher fields. However, the spectral line shapes become non-Lorenzian so FWHM can not be reliably determined for higher fields. Additional evidence of observation of spontaneous magnon decays is indicated from FWHM versus Δ_2 in Fig. 5(b), where Δ_2 is the energy difference between one magnon state and lower boundary of two-magnon continuum, the quantity which characterizes the phase space volume for the decay process.

Figure 5(c) summarizes the field dependence of the energy-integrated intensity of the experimental data plotted with the calculations by LSW. For comparison purposes, the calculated intensities were scaled by the intensity ratio of TM_{high} at zero field between data and the calculation. Clearly for TM_{low} mode, data agree well with the calculation. For TM_{high} mode, data are consistent with the calculation up to μ_0H=4 T, above which the intensity drops much faster than the calculation, suggesting the scenario of magnon breakdown. Due to the limit of maximum field accessible for the experimental study, we cannot trace down the critical field where TM_{high} mode disappears, but its trend points to a much smaller value of such a field than H_s, predicted by LSW. We also notice similar scenario of dramatic intensity change for the LM mode beyond the crossover

with the lower boundary of two-magnon continuum at 1.5 T (see Fig. 5(c)), where the crossover with the lower boundary of two-magnon continuum takes place as shown in Fig. 5(a).

With the aid of calculations by the linear spin-wave theory, our neutron scattering measurements on DLCB show the indication of field-induced magnon decays in the excitation spectra. Direct evidence for the strong repulsion between one-magon state and two-magnon continuum is renormalization of the one-magnon dispersion. Our results unambiguously establish DLCB as the first experimental realization of an ordered S=1/2 antiferromagnet that undergoes field-induced spontaneous magnon decays and our study provides much-needed experimental insights to the understanding of these spectacular quantum many-body effects in the low-dimensional antiferromagnets.

Methods

Single crystal growth. Deuterated single crystals were grown using a solution method [20]. An aqueous solution containing a 1:1:1 ratio of (DMA)Br, (35DMP)Br, where DMA$^+$ is the dimethylammonium cation and 35DMP$^+$ is the 3,5-dimethylpridinium cation, and the corresponding copper(II) halide salt was evaporated for a few days and a few drops of hydrobromic acid were added to the solution to avoid hydrolysis of the Cu(II) ion.

Neutron-scattering measurements. The high-field neutron-diffraction measurements were made on a 0.3 g single crystal with a 0.4° mosaic spread, on a triple-axis spectrometer (CTAX) at the HFIR. High-field inelastic neutron-scattering measurements were performed on a disk chopper time-of-flight spectrometer (DCS) [30] and a multi-axis crystal spectrometer (MACS) [31] at the NIST Center for Neutron Research, on two co-aligned single crystals with a total mass of 2.5 g and a 1.0° mosaic spread. At CTAX, the final neutron energy was fixed at 5.0 meV and an 11-T cryomagnet with helium-3 insert was used. At DCS, disk choppers were used to select a 167-Hz pulsed neutron beam with 3.24 meV and a 10-T cryogen-free magnet with dilution fridge insert was used. At MACS, the final neutron energy was fixed at 2.5 meV and an 11-T magnet with dilution refrigerator was used. The background was determined at T=15 K under the same instrument configuration and has been subtracted. In all experiments, the sample was oriented in the (H, H, L) reciprocal-lattice plane and the magnetic field direction is vertically applied along the [1 $\bar{1}$ 0] direction in the real space. Reduction and analysis of the data from DCS and MACS were performed by using the software DAVE [32].

Convolution with the instrumental resolution function. In comparison to the observed magnetic intensity, the calculated dynamic spin correlation function $S_\perp(\mathbf{q}, \omega)$ of spin fluctuation perpendicular to the momentum transfer $\mathbf{q}$ by LSW was numerically convolved with the instrumental resolutions function as follows:

$$I(\mathbf{q},\omega) = \int\int d\mathbf{q}'\hbar d\omega' \mathcal{R}_{\mathbf{q}\omega}(\mathbf{q} - \mathbf{q}', \omega - \omega')$$
$$\times |\frac{g}{2}F(\mathbf{q}')|^2 S_\perp(\mathbf{q}', \omega'), \qquad (5)$$

where $g \simeq 2.12$ is the Landé g-factor, $F(\mathbf{q})$ is the isotropic magnetic form factor for Cu^{2+} [33] and $\mathcal{R}_{\mathbf{q}\omega}$ is a unity normalized resolution function that is peaked on the scale of the FWHM resolution for $\mathbf{q} \approx \mathbf{q}'$ and $\hbar\omega \approx \hbar\omega'$ and approximated as a Guass distribution.

Convolution with the time-of-flight instrument resolution was considered as Gaussian broadening of the instrumental energy resolution only. Convolution with the triple-axis instrument resolution was obtained as Gaussian broadening of both instrumental energy and wave-vector resolutions, which were calculated using the Reslib software [34] in Popovici approximation [35].

Determination of the lower boundary of two-magnon continuum at finite fields. There are one acoustic and one optical transverse modes in DLCB at zero magnetic field. When a field is applied perpendicular to the easy axis, either the acoustic or the optical mode splits into two branches (TM_{high} and TM_{low}) and it becomes totally four modes. Since S_z is not a good quantum spin number in this case, the two-magnon continuum at finite field was then obtained from any combination between acoustic and optical TM_{high} and TM_{low} modes.

For the interested q=(H,H,L), which is equivalent to $(1+H,1+H,L)$, we find the lower boundary of two-magnon continuum $\varepsilon_2(\mathbf{q})^{min}$ as follows:

$$\varepsilon_2(\mathbf{q})^{min} = \varepsilon_1(\mathbf{q}_1)^{min} + \varepsilon_1(\mathbf{q}_2)^{min}, \qquad (6)$$
$$\mathbf{q} = \mathbf{q}_1 + \mathbf{q}_2, \qquad (7)$$

where ε_1 is the one-magnon dispersion relation, $\mathbf{q}_1$=(1,1,0), and $\mathbf{q}_2$=(H,H,L).

The field dependence of $\varepsilon_1(\mathbf{q}_1)^{min}$ obtained by SPINW in limit of linear spin wave approximation [23] was plotted as the yellow line in Fig. 4(a) of main manuscript. The minimum of $\varepsilon_1(\mathbf{q}_2)$ at $\mu_0 H$=0, 4, 6, and 10 T can be easily deduced from Fig. 3 of main manuscript. The determined lower boundary of two-magnon continuum at $\mu_0 H$=0, 4, 6, and 10 T was then plotted as the grey lines in Fig. 2.

Reference

* Electronic address: hongt@ornl.gov

[1] Pitaevskii, L.P. Properties of the spectrum of elementary excitations near the disintegration threshold of the excitations. Zh. Eksp. Teor. Fiz. **36**, 1168 (1959) [Sov. Phys. JETP **9**, 830 (1959)].

[2] Woods, A. D. B. & Cowley, R. A. Structure and excitations of liquid helium. Rep. Prog. Phys. **36**, 1135 (1973).

[3] Smith, A. J., Cowley, R. A., Woods, A. D. B., Stirling, W. G., & Martel, P. Roton-roton interactions and excitations in superfluid helium at large wavevectors. J. Phys. C **10**, 543 (1977).

[4] Fåk, B. & Bossy, J. Temperature dependence of $S(Q,E)$ in liquid ^{4}He beyond the roton. J. Low. Temp. Phys. **112**, 1 (1998).

[5] Stone, M. B. *et al*. Quasiparticle breakdown in a quantum spin liquid. Nature **440**, 187 (2006)

[6] Masuda, T. *et al*. Dynamics of Composite Haldane Spin Chains in IPACuCl$_3$. Phys. Rev. Lett. **96**, 047210 (2006).

[7] Plumb, K. W. *et al*. Quasiparticle-continuum level repulsion in a quantum magnet. Nat. Phys. **12**, 224 (2016).

[8] Oh, J. *et al*. Magnon Breakdown in a Two Dimensional Triangular Lattice Heisenberg Antiferromagnet of Multiferroic LuMnO$_3$. Phys. Rev. Lett. **111**, 257202 (2013).

[9] Ma, J. *et al*. Static and dynamical properties of the spin-1/2 equilateral triangular-lattice antiferromagnet Ba$_3$CoSb$_2$O$_9$. Phys. Rev. Lett. **116**, 087201 (2016).

[10] Kolezhuk, A & Sachdev, S. Magnon decay in gapped quantum spin systems. Phys. Rev. Lett. **96**, 087203 (2006).

[11] Zhitomirsky, M. E. Decay of quasiparticles in quantum spin liquids. Phys. Rev. B **73**, 100404(R) (2006).

[12] Zhitomirsky, M. E. & Chernyshev, A. L. Colloquium: Spontaneous magnon decays. Rev. Mod. Phys. **85**, 219 (2013).

[13] Zhitomirsky, M. E. & Chernyshev, A. L. Instability of antiferromagnetic magnons in strong fields. Phys. Rev. Lett. **82**, 4536 (1999).

[14] Kreisel, A., Sauli, F., Hasselmann, N., & Kopietz, P. Quantum Heisenberg antiferromagnets in a uniform magnetic field: Nonanalytic magnetic field dependence of the magnon spectrum. Phys. Rev. B **78**, 035127 (2008).

[15] Syljuåsen, O. F. Numerical evidence for unstable magnons at high fields in the Heisenberg antiferromagnet on the square lattice. Phys. Rev. B **78**, 180413 (2008).

[16] Lüscher, A. & Läuchli, A. M. Exact diagonalization study of the antiferromagnetic spin-$\frac{1}{2}$ Heisenberg model on the square lattice in a magnetic field. Phys. Rev. B **79**, 195102 (2009).

[17] Mourigal, M., Zhitomirsky, M. E., & Chernyshev, A. L. Field-induced decay dynamics in square-lattice antiferromagnets. Phys. Rev. B **82**, 144402 (2010).

[18] Fuhrman, W. T., Mourigal, M., Zhitomirsky, M. E., & Chernyshev, A. L. Dynamical structure factor of quasi-two-dimensional antiferromagnet in high fields. Phys. Rev. B **85**, 184405 (2012).

[19] Masuda, T. *et al*. Instability of magnons in two-dimensional antiferromagnets at high magnetic fields.

Phys. Rev. B **81**, 100402 (2010).

[20] Awwadi, F., Willett, R. D., Twamley, B., Schneider, R., & Landee, C. P. Strong rail spin 1/2 antiferromagnetic ladder systems: (Dimethylammonium)(3,5-Dimethylpyridinium)CuX$_4$, X = Cl, Br. Inorg. Chem. **47**, 9327 (2008).

[21] Hong, T. *et al.* Magnetic ordering induced by interladder coupling in the spin-1/2 Heisenberg two-leg ladder antiferromagnet C$_9$H$_{18}$N$_2$CuBr$_4$. Phys. Rev. B **89**, 174432 (2014).

[22] Aoyama, C. *et al.* unpublished.

[23] Toth, S. & Lake, B. Linear spin wave theory for single-Q incommensurate magnetic structures. J. Phys. Condens. Matter **27**, 166002 (2015).

[24] Affleck, I. & Wellman, G. F. Longitudinal modes in quasi-one-dimensional antiferromagnets. Phys. Rev. B **46**, 8934 (1992).

[25] Lake, B., Tennant, D. A., & Nagler, S. E. Novel Longitudinal Mode in the Coupled Quantum Chain Compound KCuF$_3$. Phys. Rev. Lett. **85**, 832 (2000).

[26] Rüegg, Ch. *et al.* Quantum magnets under pressure: controlling elementary excitations in TlCuCl$_3$. Phys. Rev. Lett. **100**, 205701 (2008).

[27] Normand, B. & Rice, T. M. Dynamical properties of an antiferromagnet near the quantum critical point: application to LaCuO$_{2.5}$. Phys. Rev. B **56**, 8760 (1997).

[28] Hong, T *et al.* Effect of pressure on the quantum spin ladder material IPA-CuCl$_3$. Phys. Rev. B **78**, 224409 (2008).

[29] Hong, T *et al.* Neutron scattering study of a quasi-two-dimensional spin-1/2 dimer system: Piperazinium hexachlorodicuprate under hydrostatic pressure. Phys. Rev. B **82**, 184424 (2010).

[30] Copley, J. R. D. & Cook, J. C. The disk chopper spectrometer at NIST: a new instrument for quasielastic neutron scattering studies. Chem. Phys. **292**, 477 (2003).

[31] Rodriguez, J. A. *et al.* MACS-a new high intensity cold neutron spectrometer at NIST. Meas. Sci. Technol. **19**, 034023 (2008).

[32] Azuah, R. T. R. M. DAVE: A comprehensive software suite for the reduction, visualization, and analysis of low energy neutron spectroscopic data. J. Res. Natl. Inst. Stan. Technol. **114**, 341 (2009).

[33] Brown, P. J. *et al.* Magnetic form factors, Chapter 4.4.5, International Tables for Crystallography vol. C.

[34] Zheludev, A. ResLib 3.4c (2007)

[35] Popovici, M. On the resolution of slow-neutron sepctrometers. IV. The triple-axis spectrometer resolution function, spatial effects included. Acta Cryst. **A31**, 507 (1975).

Acknowledgments

Author contributions

T.H. conceived the project. F.F.A. and M.M.T. prepared the samples. T.H., H.A., and Y.Q. performed the neutron-scattering measurements. T.H., A.L.C., M.M., D.A.T., K.C., and K.P.S. analysed the data. All authors contributed to the writing of the manuscript.

Additional information

Competing financial interests: The authors declare no competing financial interests.

Materials & Correspondence. Correspondence and requests for materials should be addressed to T.H. (email: hongt@ornl.gov).

* Electronic address: hongt@ornl.gov